NANO EXPRESS

In Situ Confocal Raman Mapping Study of a Single Ti-Assisted ZnO Nanowire

Ashish C. Gandhi · Hsuan-Jung Hung · Po-Hsun Shih ·
Chia-Liang Cheng · Yuan-Ron Ma · Sheng Yun Wu

Abstract In this work, we succeeded in preparing in-plane zinc oxide nanowires using a Ti-grid assisted by the chemical vapor deposition method. Optical spatial mapping of the Confocal Raman spectra was used to investigate the phonon and geometric properties of a single ZnO nanowire. The local optical results reveal a red shift in the non-polar E_2 high frequency mode and width broadening along the growth direction, reflecting quantum-confinement in the radial direction.

Introduction

One-dimensional nanostructures, such as nanowires (NWs), nanorods, nanobelts and nanoparticles have become the focus of intensive research in the twentyfirst century due to their unique applications in microscopic physics and for the fabrication of nanoscale devices [1–6]. Recently, a variety of novel devices including nanoscale lasers, electrochemical gated quantum dot transistors have been investigated. The highly efficient exciton UV lasing action under optical pumping from the nano-clusters and thin films make for an exceptionally important semiconductor. The wide band gap (~ 3.37 eV) and large excitation binding energy (~ 60 meV) at room temperature of zinc oxide (ZnO) make it a very promising material for nanoscale optoelectronic applications [7–11]. The availability of large quantities of well-aligned ZnO nanowires (ZnONWs) in a single crystalline form is extremely important for the development of high-efficiency, short-wavelength optoelectronic nano-devices. However, very little is known about the optical vibrational spectra of ZnO nanorods, except that the vibrational frequencies are expected to be different from the bulk material, since a large quantity of the bonding partners are missing at the surface [12]. Raman scattering is a very useful nondestructive technique for examination of phononic behavior, providing information about the crystal structure, lattice dynamics and defects. Recently, Raman scattering has been used to investigate individual carbon nanotubes [13], SiC nanowires [14] and ZnO belts [15]. In the present study, we report on the quantum confined effects in a single ZnONW using in situ confocal Raman mapping technique. Comprehensive structural analysis shows that these ZnONWs are single crystal in nature with excellent crystal quality.

Experimental Details

The various possible crystalline ZnO nanostructures, including nanowires, nanoneedles and nanorods, have been synthesized using a verity of techniques such as the hydrothermal process, the microwave-assisted aqueous route, thermal evaporation, nano-imprint techniques, vapor phase transport, thermal decomposition microemulsion, ultrasonic spray pyrolysis, molecular beam epitaxy and the laser ablation technique [2, 16–21]. However, well-aligned and c-axis-oriented nanowires must be grown either on epitaxial matched substrates and/or using catalytic templates, mostly at high processing temperatures (~ 900°C). The mismatch between the coefficient of thermal expansion of

A. C. Gandhi · H.-J. Hung · P.-H. Shih · C.-L. Cheng ·
Y.-R. Ma · S. Y. Wu (✉)
Department of Physics, National Dong Hwa University,
Hualien 97401, Taiwan
e-mail: sywu@mail.ndhu.edu.tw

(a) Concept of Chemical Vapor Deposition

The fabrication process of ZnONWs
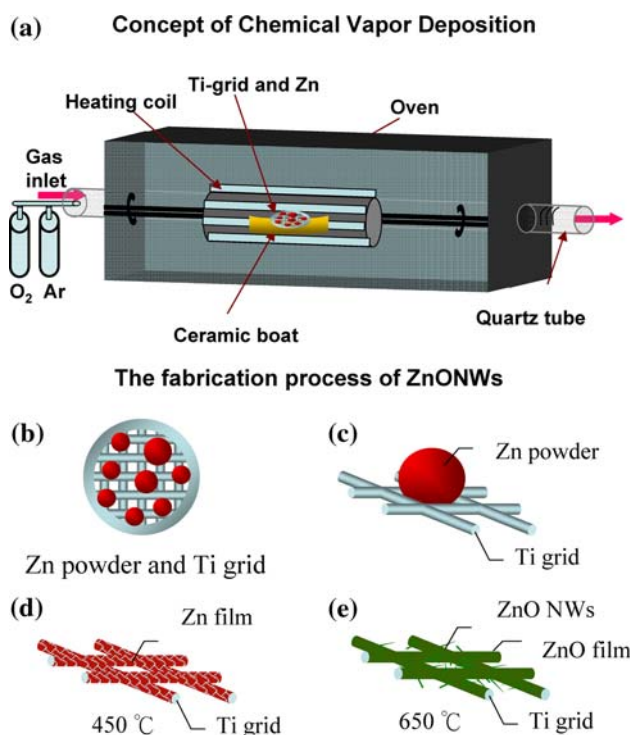
Fig. 1 a Conceptual diagram of the chemical vapor deposition process in which Zn is placed on a Ti grid. The ZnONW fabrication process: **b**, **c** Zn powder on the Ti-grid; **d** the formation of a Zn film on a Ti-grid; and **f** fully grown ZnONWs

the nanorods and the substrate must be reduced when they are deposited. The presence of a catalytic layer of another material during the synthesis of the nanostructures may lead to contamination of the grown material, especially at the edges of the nanostructures. Therefore, synthesis of nanostructures without a catalytic template, or using the self-catalytic behavior of the material would be of interest. So, to solve these problems, a new one-step growth method is developed using the chemical vapor deposition (CVD) process, as shown in Fig. 1a. A Ti-grid is used as a substrate so that Ti replaces gold as the site for further ZnO nanowire growth. Some amount of 99.9% pure Zn powder was placed on the Ti-grid, mounted using a ceramic boat, as shown in top view of Fig. 1b and side view of Fig. 1c, respectively. The whole was then inserted into a quartz tube and placed in close proximity to the middle of the furnace. Since Zn and Ti have very similar physical properties and particularly the crystalline properties like both have same hexagonal type of crystal structure and the coefficient of linear expansion value differ slightly from each other. In this method i.e., the Ti-grid assisted CVD method, both Ti and Zn have the same space group, $P6_3/mmc$ (No:194) and there is limited mismatch of lattice constants. Ti-grid can assist the growth of c-axis oriented ZnONWs up to a long range of temperature because the

melting point of Ti is 1,668°C which is very higher than melting point of Zn. Therefore by using Ti as a substrate we can avoid impurity of Ti in ZnONWs at lower temperatures (<1,668°C) and also due to any catalytic-template as there is no need now. The synthesis was performed in two steps: 1. the first step was heating the quartz furnace to about 450°C for 1 h to melt the Zn in a vacuum. This resulted in a uniform Zn thin film on the Ti-grid, as shown in Fig. 1d; 2. in the second step the sample was maintained at a temperature of 650°C for 2 h in a mixed argon (Ar) (100 *sccm*) and oxygen (O$_2$) flow after which it was allowed to cooled down naturally. The pressure was kept at about 100 Torr by a mass flow controller. The length and mean diameter of ZnONWs can also be adjusted by controlling the level of the vacuum and the working pressure. The forming of in-plane ZnONWs can be detected by the confocal Raman scattering, giving us direct observations with which to investigate the shifting of the phonon mode of the quantum confinement effects. The applicability of investigating the quantum confinement of a single nanowire without any preparation for different sizes of nanoparticles is possible because the detection is relatively straightforward and the reproduced Raman signals can be observed.

Results and Discussion

Morphology and SEM Images of ZnONWs

The morphology and structure of the resultant ZnONWs (Fig. 1e) were then be characterized by scanning electron microscopy (SEM) and transmission electron microscopy (TEM). SEM image observations were made using a SM-71010 microscope (JEOL, Japan). The SEM images of the as-grown ZnO nanorod array are shown in Fig. 2a, b. It can be seen that the ZnONWs grew homogeneously on the Ti-grid substrate to form straight nanowires. Observation of the uniform nanowires (with lateral dimensions, on the order of nms i.e., in the hundred- to ten-nano-scale), show that they grew up to a few microns in length. The corresponding distribution of the diameters of the ZnONWs is shown in the inset to Fig. 2a. The solid lines represent the fitting curves assuming log-normal functions. The log-normal distribution is defined as follows: $f(d) = \frac{1}{\sqrt{2\pi}d\sigma}\exp\left(-\frac{(\ln d-\ln <d>)^2}{2\sigma^2}\right)$, where $<d>$ is the mean value and σ is the standard deviation of the function. The diameter of a ZnONW ranges from 90 to 170 nm. The length of the ZnONWs was found to be dependent on the deposition time. In the present work, we succeeded in growing ten μm-long nano-wires (NWs) within ∼120 min. The mean diameters obtained from the fits of log-normal
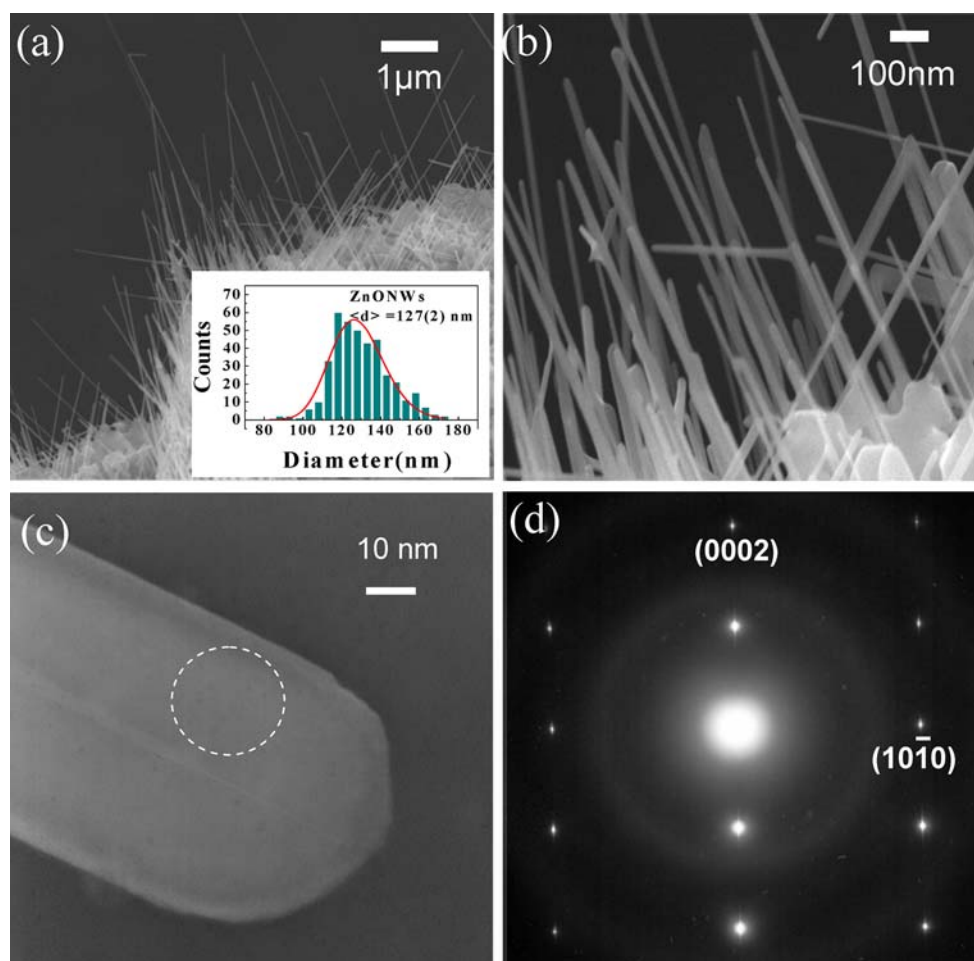
Fig. 2 SEM images of single crystal ZnONWs on Ti-grids at magnifications of: **a** 10,000; and **b** 50,000. **c** High-resolution TEM images of a single crystal ZnONW along with; **d** selection area electron diffraction pattern of ZnONW

distribution are $<d> = 127(2)$ nm. The small standard deviation ($\sigma = 0.11$) of the function indicates that the distribution is confined to a limited range, and it can be seen that the broadened width of the distribution profile is due to the crystalline effects. The TEM image of a selected single isolated ZnONW (Fig. 2c) was obtained from a JEM-3010 microscope (JEOL, Japan) and can be used to study the crystalline structure. Figure 2d shows the selected area electron diffraction (SAED) patterns for the circled area in Fig. 2c which were taken along the [010] zone axis. The clear, sharp diffraction spots observed are indicative of the good single-crystalline structure of the ZnONWs. The reflections correspond to (0001), (0002) and ($10\bar{1}0$) lattice planes of ZnO with indexed hexagonal structure, which is in good agreement with previously reported results [10]. The experimental results indicate that without choosing any specific direction oriented planes of Ti as a substrate, there is still growth of ZnO in the *c*-axis direction which results in uniform and crystalline ZnONWs.

Confocal Raman Scattering

Confocal Raman scattering is a technique which is so highly sensitive to submicron spatial resolution that it can, under optimum conditions, take measurements with a resolution corresponding to half the wavelength of the exciting light $\lambda/2$. This high spatial resolution gives it great advantages for examining the quantum confinement effects along a single nanowire. The spectroscopic properties of individual ZnONWs as evidenced by the Confocal Raman spectra from a spectrometer (Alpha 300 WiTec) equipped with a piezo scanner and $\times 100$ microscope objectives (n.a. $= 0.90$; Nikon) were investigated. A single ZnONW sample was excited with a 488 nm Ar ion laser (Melles Griot) (5 mW laser power), to form a spot ~ 0.3 μm in diameter, giving a power density of ~ 100 W cm^{-2}. No noticeable difference in Raman shifts was found due to the effects of laser annealing. The ZnONW wurtzite structures belong to the *P6₃mc* space group, with two formula units

per primitive cell, where all atoms occupy C_{3v} sites. Group theory predicts the Raman active zone-centers of the optical phonons predicted to be $A_1 + 2E_2 + E_1$. The phonons having A_1 and E_1 symmetry are polar phonons and, hence, the transverse-optical (TO) and longitudinal-optical (LO) phonons exhibit different frequencies. Nonpolar phonon modes with symmetry E_2 have two frequencies: E_2(high) is associated with oxygen atoms and E_2(low) is associated with the Zn sublattice. All described phonon modes have been reported in the Raman-scattering spectra of bulk ZnO [22]. In order to obtain a good interpretation of this experimental data and avoid uncertainties, Confocal Raman spectroscopy was performed on a single ZnONW at room temperature, recording backscattering geometries with no polarization direction. Figure 3a, b show the Confocal Raman scattering spectra of single ZnONWs grown on a Ti-grid and on ZnO powder for comparison. The main peak at 435.8 cm^{-1} is assigned to the E_2 (high frequency) optical phonon mode of ZnO, taken from the optical image of a single ZnONW (marked as B) and presented in the inset to Fig. 3a [23]. The weak and broad peak at 332.5 cm^{-1} is assigned to the second-order Raman spectrum arising from the E_2 (high)–E_2 (low) multiple phonons scattering process of ZnO [24]. A comparison of the Raman spectra for the ZnO powder [22] shows an obvious shift in the E_2 (high) phonon mode of ZnONW to a low frequency. The peak width is broadened as a result of the nano-size effect. The nonploar behavior of the E_2 mode did not result in any noticeable change in the incident polarization vector, which makes this a good
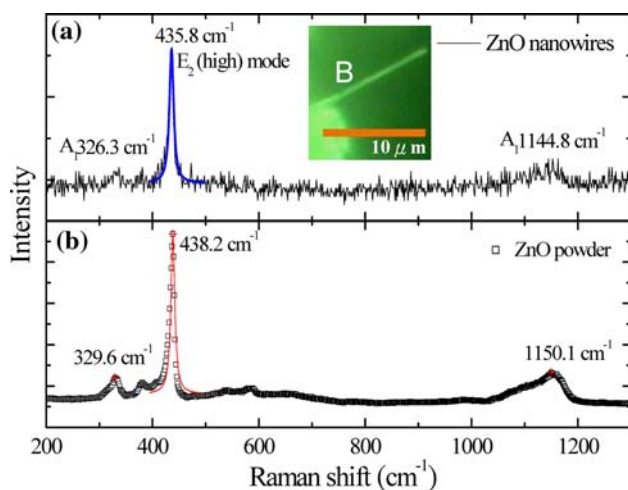
Fig. 3 **a** Confocal Raman spectra of ZnONW; and **b** ZnO powders. The main peak at 435.8 cm^{-1} is assigned to the E_2 (high frequency) optical phonon mode of ZnO. The inset shows an optical image of a single isolated ZnONW for confocal Raman scattering. The Lorentzian curves fitting results show that the values of peaks and full width half maximum (FWHM) are 435.8(2) and 9.51(1) cm^{-1} for a single ZnONW and 438.2(1) and 9.12(2) cm^{-1} for the ZnO powder, respectively
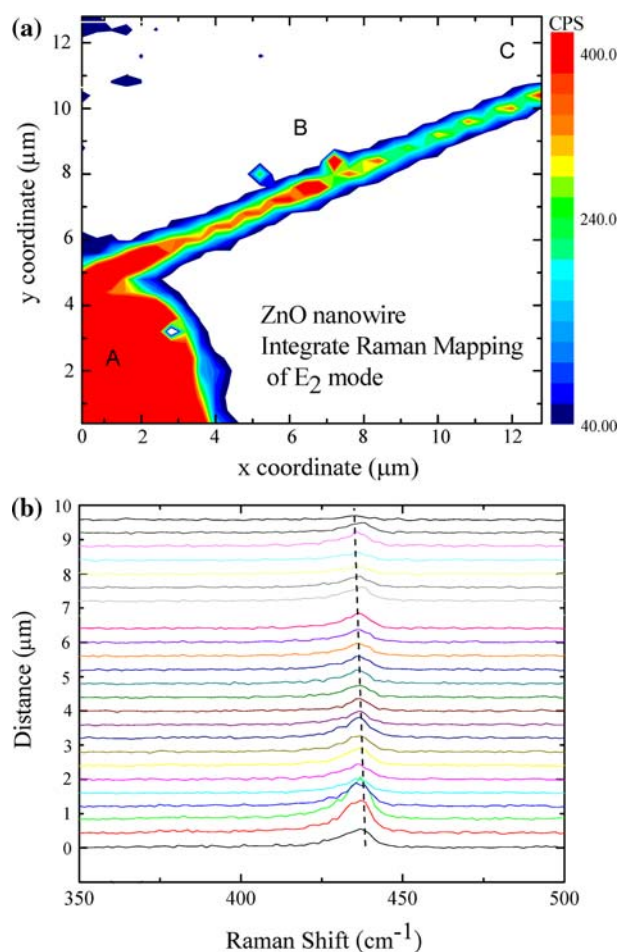
Fig. 4 **a** Spatial mapping of corresponding Raman intensities of the E_2 peak ranging from 417 to 448 cm^{-1}; **b** series of Raman spectra taken along the growth direction of a single ZnONW. The E_2 phonon peak shifts to a lower frequency and broadens as a result of the nano-sized effect

candidate in order to study the interplay between the local phonon behavior and geometric anisotropy of a single ZnONW using the in situ Confocal Raman mapping technique.

The Raman intensities corresponding to the E_2 peak (obtained by intensity integration with the phonon mode ranging from 417 to 448 cm^{-1}) are mapped and displayed in Fig. 4a for a 12×12 μm^2 area. Different colours are used to differentiate the intensity of the peak and allow direct visualization of the spatial distribution of Zinc oxide in a single ZnONW. The red area of the substrate (marked A) reflects the existence of ZnO film in the Ti-grid. The decrease in the integrated intensity distribution along the growth direction of ZnONW less than 6 μm in length (marked B) reveals that it is likely that the nanowire formation proceeds through the nucleation of ZnO$_x$ and ZnO and that a boundary transition occurred during the growth process. The formation of a single zinc oxide nanowire is

attributed as due to crystallization from the Zn/ZnO mixed phase to form the ZnO structure. As the diameter decreases, the surface roughness also increases, due to an increase in the surface effect for smaller diameters of a single nanowire. The intensity distribution decreases by a factor of 2 when the length of the nanowire exceeds 6 μm (marked B). This takes place through crystallization from the ZnO_x/ZnO mixed phase to form a pure ZnO structure. The SEM image results show that as prepared, the ZnONWs have diameters in the nano-range and lengths up to the micro-range, where the length is greater than the diameter, which means that the quantum confinement effect mainly occurs along the diameter of the ZnO. Figure 4b shows the Raman spectra taken from a series of Raman scans along the sample wire. The E_2 phonon mode in a single ZnONW will shift to a lower frequency and the peak will be broadened as a result of the nanosized effect. It is known that the plane wave in ideal long range crystals of $K = 0$ momentum selection rule is satisfied in the first order Raman spectra. When the dimensionality is reduced to one, the phonon scattering will not be limited to the center of the Brillouin zone and the effect of phonon dispersion near the zone center must be considered, resulting in the red shift, broadening, and the asymmetry of the vibration mode.

Two-Dimensional Raman Mapping and Analysis

The distance dependence of the E_2 phonon linewidth and intensity obtained from the two-dimensional Raman images of a single ZnONW are shown in Fig. 5a, b. The plots help to visualize the detailed phonon structure of the E_2 mode. The profile analysis can be described by the algorithm suggested by Campbell et al. [25]. The original Raman image shown at the top of Fig. 5 gives direct information about changes in intensity and line width along the growth direction. Figure 5a shows a plot of the line width. The slight fluctuation in line width below ~ 2.2 μm is due to crystallization from the Zn/ZnO mixed phase. After ~ 2.2 μm, the line width increases slightly up to ~ 8.5 μm. To further characterize and quantity the dependency of linewidth on length we can use the phonon–phonon scattering function. This can be well described as $\Gamma(x) = \Gamma_o + a \exp\frac{x}{L_c}$, where Γ_o is the linewidth of the optical mode at an initial point; L_c is the critical phonon length; and a is the coefficient. The linewidth of a phonon line is a measure of phonon scattering. The solid line in Fig. 5a represents the linewidth function. A significant increase along the growth direction is found from the fitting, revealing the characteristic 1D nature of a nanowire. The line width approaches to slack below $x = 2.1(5)$ μm, and its magnitude is extrapolated to $\Gamma_o = 9.1(5)$ cm^{-1} for
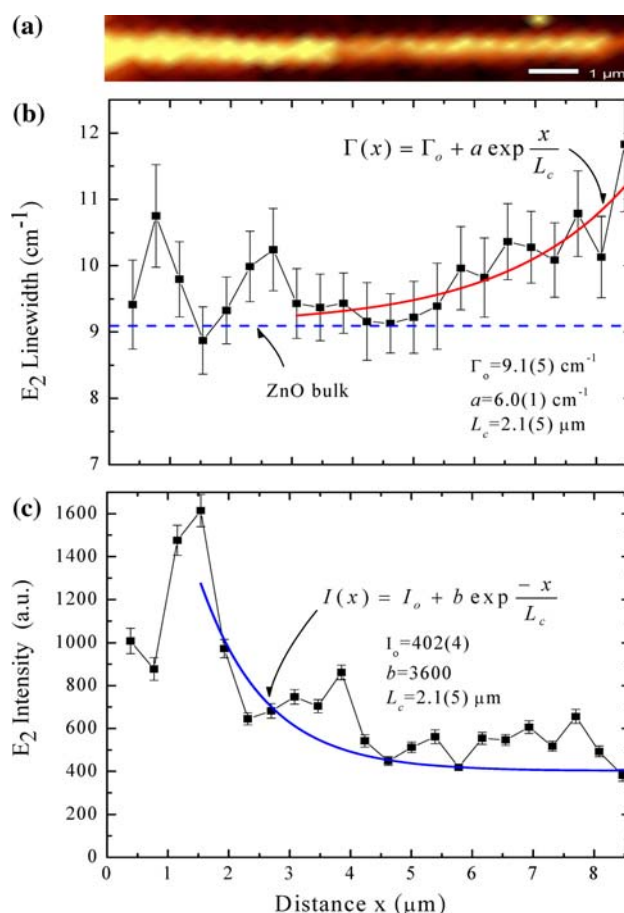
Fig. 5 a The line width along the length of ZnONW; and **b** the peak intensity along the length of ZnONW which decreases with increasing length

the ZnO nanowires. It is noteworthy that the value of Γ_o falls to 9.1(5) cm^{-1}, which is close to the instrumental function full width half maximum (FWHM) measured for the ZnO powder ($\Gamma_o = 9.12(2)$ cm^{-1}; see the dash curve indicated in blue). Figure 5b shows a plot of intensity along the length of the ZnONW. The results indicate that the intensity continues to decrease along the growth direction toward the tip, following the expression $I(x) = I_0 + b \exp\frac{-x}{L_c}$, where $I_o = 402(4)$ and $b = 3600(500)$ (a.u.). The intensity decreases because: we can see that the tip volume of a single nanowire is smaller than that of the root volume and the intensity of Raman scattering is directly proportional to the number of centers present in the volume illuminated by the laser beam. In addition, while the objective of Raman spectroscopy is to scan along the sample wire, this individual wire may not be parallel to the scanning direction. A tilted wire could de-focus the collection of scattered light resulting in some decrease in the intensities of the peak. It worth noting that, since the change in laser power does not lead to any changes in the E_2(high) phonon mode, and the local temperature

calculated for the maximum laser power of 20 mW is less than 60°C, it is clear that local heating cannot be responsible for the shift and broadening of the E_2(high) phonon mode. Furthermore, apart from the quantum confinement effect, the other contribution of broadening and shift of peak can also be explained as due to oxygen deficiencies and residual stresses. It has been discussed in previous reports of single-crystalline ZnO [26] and TiO$_2$ nanowires [27]. It was worth to note that if the growth time of ZnONW was reduced using CVD method, the mean diameter of ZnONW would also be decreased. A stronger red shift will be expected in E_2 mode, following the phenomenological phonon confinement model proposed by Richter et al. (RWL model) [28] and the bond polarizability model offered by Zi et al. [29, 30]. These two models can be used to explain the peak shift and broadening observed in nano-scale nanowires, where the shift evolution is corrected to the reduction of the diameter only. It has been observed and discussed in previous reports of tip-like single CuO nanowires [31]. Further theoretical and experimental studies that focus on the diameter dependency of Raman phononic modes generated in a tip-like ZnO nanowire may help to identify the mechanisms that associated with the strong Raman shifts in ZnO nanowire.

Conclusion

The chemical vapor deposition (CVD) technique was used to grow single crystalline ZnONWs on a Ti-grid with a hexagonal cross-section without using any catalyst at 650°C. The experimental results indicate that, without choosing any specific direction for the orientation of the Ti substrate, there is still growth of ZnO in a *c*-axis direction that results in uniform and crystalline ZnONWs. Confocal Raman scattering was performed to study the phonon behavior and geometric anisotropy of a single ZnONW. As the diameter along the growth direction is reduced, the peak position and linewidth of the non-polar E_2 (high) mode resulted in red shift, broadening, and asymmetry of the peak profile. The results reveal the local optical behavior and the uniformity of crystal growth, confirming that the quantum-confinement in the radial direction is in agreement with the theoretical calculations [25].

References

1. Z.L. Wang, J. Phys. Condens. Mater. **16**, 829 (2004)
2. M.H. Huang, S. Mao, H. Feick, H. Yan, Y. Wu, H. Kind, E. Weber, R. Russo, P. Yang, Science **292**, 1897 (2001)
3. G.Z. Xing, J.B. Yi, J.G. Tao, T. Liu, L.M. Wong, Z. Zhang, G.P. Li, S.J. Wang, J. Ding, T.C. Sum, C.H.A. Huan, T. Wu, Adv. Mater. **20**, 3521 (2008)
4. Z. Zhang, Y.H. Sun, Y.G. Zhao, G.P. Li, T. Wu, Appl. Phys. Lett. **92**, 103113 (2008)
5. S.C. Minne, S.R. Manalis, C.F. Quate, Appl. Phys. Lett. **67**, 3918 (1995)
6. Z. Zhang, S.J. Wang, T. Yu, T. Wu, J. Phys. Chem. C **111**, 17500 (2007)
7. H. Kind, H. Yan, B. Messer, M. Law, P. Yang, Adv. Mater. **14**, 158 (2002)
8. J.M. Bao, M.A. Zimmler, F. Capasso, X.W. Wang, Z.F. Ren, Nano Lett. **6**, 1719 (2006)
9. M.C. Jeong, B.Y. Oh, M.H. Ham, J.M. Myoung, Appl. Phys. Lett. **88**, 202105 (2006)
10. A. Qurashi, N. Tabet, M. Faiz, T. Yamzaki, Nanoscale Res. Lett. **4**, 948 (2009)
11. K. Keem, H. Kim, G.T. Kim, J.S. Lee, B. Min, K. Cho, M.Y. Sung, S. Kim, Appl. Phys. Lett. **84**, 4376 (2004)
12. V.A. Fonoberov, A.A. Baladin, Phys. Rev. B **70**, 233205 (2004)
13. A.V. Naumov, O.A. Kuznetsov, A.R. Harutyunyan, A.A. Green, M.C. Hersam, D.E. Resasco, P.N. Nikolaev, R.B. Weisman, Nano Lett. **9**, 3203 (2009)
14. J. Frechette, C. Carraro, J. Am. Chem. Soc. **128**, 14774 (2006)
15. S. Singamaneni, M. Gupta, R. Yang, M.M. Tomczak, R.R. Naik, Z.L. Wang, V.V. Tsukruk, ACS Nano **3**, 2593 (2009)
16. V.A.L. Roy, A.B. Djurisic, W.K. Chan, J. Gao, H.F. Lui, C. Surya, Appl. Phys. Lett. **83**, 141 (2003)
17. A.L. Roest, J.J. Kelly, D. Vanmaekelbergh, E.A. Meulenkamp, Phys. Rev. Lett. **89**, 036801 (2002)
18. Z.W. Pan, Z.R. Dai, Z.L. Wang, Science **291**, 1947 (2001)
19. X. Wang, Q. Li, Z. Liu, J. Zhang, Z. Liu, R. Wang, Appl. Phys. Lett. **84**, 4941 (2004)
20. B. Min, J.S. Lee, J.W. Hwang, K.H. Keem, M.I. Kang, K. Cho, M.Y. Sung, S. Kim, M.S. Lee, S.O. Park, J.T. Moon, J. Cryst. Growth **252**, 565 (2003)
21. J. Volk, T. Nagata, R. Erdélyi, I. Bársony, A.L. Tóth, I.E. Lukács, Z. Czigány, H. Tomimoto, Y. Shingaya, T. Chikyow, Nanoscale Res. Lett. **4**, 699 (2009)
22. N. Ashkenov, B.N. Mbenkum, C. Bundesmann, V. Riede, M. Lorenz, D. Spemann, E.M. Kaidashev, A. Kasic, M. Schubert, M. Grundmann, G. Wagner, H. Neumann, J. Appl. Phys. **93**, 126 (2003)
23. J. Serrano, A.H. Romero, F.J. Manjon, R. Lauck, M. Cardona, A. Rubio, Phys. Rev. B **69**, 094306 (2004)
24. A. Umar, S.H. Kim, Y.–.S. Lee, K.S. Nahm, Y.B. Hahn, J. Cryst. Growth **282**, 131 (2005)
25. I.H. Campbell, P.M. Fauchet, Solid State Commun. **58**, 739 (1986)
26. H.T. Ng, B. Chen, J. Li, J. Han, M. Meyyappan, J. Wu, S.X. Li, E.E. Haller, Appl. Phys. Lett. **82**, 2023 (2003)
27. Y. Lei, L.D. Zhang, J.C. Fan, Chem. Phys. Lett. **338**, 231 (2001)
28. H. Richter, Z.P. Wang, L. Ley, Solid State Commun. **39**, 625 (1981)
29. J. Zi, K. Zhang, X. Xie, Phys. Rev. B **55**, 9263 (1997)
30. J. Zi, H. Bucher, C. Faller, W. Ludwig, K. Zhang, X. Xie, Appl. Phys. Lett **69**, 200 (1996)
31. M.H. Chou, S.B. Liu, C.Y. Huang, S.Y. Wu, C.–.L. Cheng, Appl. Surf. Sci. **254**, 7539 (2008)